JOURNAL OF MATERIALS SCIENCE **38** (2003) 4353–4363

Amorphous ferroelectric thin film capacitive device for hydrogen detection

O. K. TAN, X. F. CHEN, W. ZHU*
Microelectronics Centre, School of Electrical and Electronic Engineering, Nanyang Technological University, Nanyang Avenue, Singapore 639798
E-mail: ewzhu@ntu.edu.sg

Hydrogen is a promising alternative energy source for next generation automobile engines that meet the concern of energy shortage and global environmental pollution. Hydrogen detection is an important associated technology to be developed. The recently developed amorphous ferroelectric thin film capacitive gas sensors with a largely improved sensitivity to hydrogen show a great potential for this associated technology. This review presents an overall picture of amorphous ferroelectric thin film hydrogen gas sensors. It focuses on the correlation among processing, microstructural evolution and electrical properties of amorphous ferroelectric thin films. An attempt is made to detail the hydrogen sensitivity and transient response of various prototype capacitive devices with respect to the quality of the films and the hydrogen kinetic processes in the Pd/ferroelectric heterostructure. Recent advances on the hydrogen interface-blocking model for amorphous ferroelectric gas sensors are also described.

1. Introduction

With the steady increase in gasoline consumption and awareness of global environmental pollution, there have been substantial research and development activities in seeking substitutional energy sources for existing automobile engines using fossil fuel. Among them, hydrogen is a promising candidate owing to its high combustion efficiency. Hydrogen has the highest energy content per unit mass of 41.9 MJ/kg, almost three times higher than gasoline, and a wide flammability range of 5 to 75 vol% in air as well. It is also a clean fuel, emitting no greenhouse gases, ozone layer depleting chemicals, and acid rain ingredients and associated pollution. Although hydrogen is potentially less hazardous, some of its characteristics could theoretically make it more dangerous in certain applications. The technological development for the safety and economical transportation and storage is desired before it is realized as a major alternative energy source.

Nowadays, hydrogen leakage detection is being developed generally based on the state-of-the-art solid-state and photonics technologies [1, 2], and several devices have been commercialized. The initial solid-state gas sensor, having simple, small size and low-cost structure, could be backdated to the hydrogen-sensitive metal-oxide-semiconductor field effect transistor (MOSFET) proposed by Lundström and Svensson in 1975 [3, 4]. The general physical description of such semiconductor devices with catalytic metal gates based on the metal-insulator interface has been well established [2, 5–8]. Seeking novel dielectric layer for further improvement is still in progress, for example, Si_3N_4 [9], Ta_2O_5 [9], Al_2O_3-SiO_2 [5], Al_2O_3 [10, 11], SiO_2-SiC [12, 13], SiC [14], ZnO [15], TiO_2 [16], GaAs [17], and diamond thin film [18, 19].

In 1998, a considerably improved sensitivity for hydrogen gas detection was achieved by Zhu *et al.* [20, 21] using a sol-gel ferroelectric $Ba_{0.67}Sr_{0.33}Ti_{1.02}O_3$ (BST) thin film in amorphous state. In their studies, a prototype Pd/BST/Pt capacitive device was fabricated, and the voltage shift due to the presence of hydrogen at 1000 ppm as high as 4.5 V was measured, which is about 7 times larger than the best value reported in literature [9–19]. Such voltage shift is believed to originate from the high dielectric constant of amorphous BST thin films, which would enhance the dipolar polarization potential at the Pd/BST interface in presence of hydrogen ions. A similar hydrogen-sensitive conduction behavior was reported in a Pd/amorphous PZT film/Pt capacitive device by Deng *et al.* [22]. These successes in metal-ferroelectric-metal (MFM) capacitive devices show great promise in fabricating monolithic Si-based ferroelectric thin film gas sensors and open a new area of application for ferroelectrics. To distinguish from other dielectric thin films, they are called *amorphous ferroelectric thin film* since they are commonly referred to ferroelectric materials in crystal state. This review focuses on recent advances in hydrogen-sensitive behaviors of ferroelectric thin film capacitors, related mechanism, and feasibility for hydrogen gas sensor application.

* Author to whom all correspondence should be addressed.

2. Fabrication of amorphous ferroelectric films for hydrogen detection

To date, two conventional thin film techniques, sol-gel and RF sputtering, have been used to fabricate amorphous ferroelectric thin films for hydrogen detection. To meet the requirement of gas sensing devices, much attention has been paid to the microstructural optimization to achieve lower leakage current and higher dielectric breakdown field.

A comprehensive study on the sol-gel process and microstructural evolution of amorphous BST thin film hydrogen gas sensors with low leakage current has been summarized by Zhu *et al*. [23–25]. The amorphous structure is essential to effectively stop the diffusion of hydrogen into the films, whereas polycrystalline perovskite shows an open structure for hydrogen diffusion [26–28]. To achieve the amorphous structure, annealing temperature is crucial in thin film fabrication. Fig. 1 illustrates a typical thermal decomposition process of the barium strontium titanate $(Ba_{0.67}Sr_{0.33})Ti_{1.02}O_3$ xerogel. The endothermic peak at 77°C is due to the evaporation of ethanol in the sol-gel solution. The exothermic peaks at 340 and 361°C are accordingly correlated to the decomposition of $BaCO_3$ and $SrCO_3$, which may easily form at relatively low temperatures in the heating process, and those at 444 and 586°C are attributed to be the glass transition and crystallization temperature, respectively. Thus, the pyrolyzed $(Ba,Sr)TiO_3$ thin film should be subjected to a post heat-treatment in a narrow temperature range just above the glass transition point at 444°C. Fig. 2 presents the phase evolution in $(Ba_{0.67}Sr_{0.33})Ti_{1.02}O_3$ thin film by varying post-annealing temperatures. It is clear that for the film annealed at 475°C, which is just a little bit above the glass transition temperature of 444°C, the curve (c) is virtually the same as that of curve (a) for the Pt coated Si substrate, indicating that the film has the amorphous nature. On further increasing the annealing temperatures, the $(Ba,Sr)TiO_3$ perovskite phase is developed, as shown in curve (d) for annealing temperature of 575°C and (e) of 675°C, respectively. A further microstructural study was carried out using high-resolution transmission electron microscopy (TEM) shown in Fig. 3 [25]. From the lattice images and electron diffraction patterns, it is evident that the film annealed at 475°C has an amorphous structure, while the film annealed at 600°C has its polycrystalline phase and relatively open grain boundaries. In fact, structural evolution might affect their electrical properties accordingly. Room temperature *I-V* characterization [29] suggests that an excellent *I-V* character is achieved for the amorphous BST thin film annealed at 475°C, giving a typical electrical insulating behavior of amorphous ferroelectric materials. At an annealing temperature of 400°C, organic residues in the films result in an unstable leaky *I-V* behavior. Further increase in the annealing temperature to 600 and 650°C causes the films to form polycrystalline growth of the grains, and exhibit higher leakage currents.

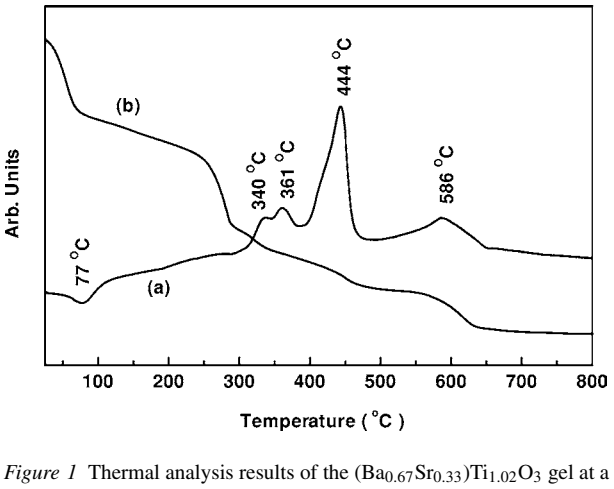

Figure 1 Thermal analysis results of the $(Ba_{0.67}Sr_{0.33})Ti_{1.02}O_3$ gel at a heating rate of 2°C/min in air: (a) DTA and (b) TGA [20].

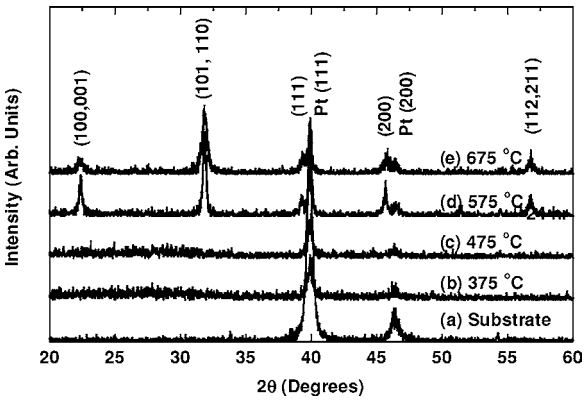

Figure 2 XRD patterns of the Pt-coated Si substrate (a) and of $(Ba_{0.67}Sr_{0.33})Ti_{1.02}O_3$ films annealed for 1 h in air at (b) 375°C (as-pyrolyzed), (c) 475°C, (d) 575°C and (e) 675°C [20].

In comparison, Tan *et al*. [30] and Chen *et al*. [31, 32] also prepared amorphous $(Ba,Sr)TiO_3$ thin film gas sensors using magnetron co-sputtering process and investigated their microstructural evolution by changing deposition temperature. It is identified that the films are amorphous when deposited at a temperature below 300°C. The polycrystalline perovskite grains in the films start to grow at 350°C, and the grains grow gradually with increasing deposition temperature. TEM observation indicates that the BST film deposited at 300°C is composed of a crak-free amorphous phase. While increasing the deposition temperature up to 500°C, the BST film mainly exhibits a columnar structure, which is composed of fine polycrystal grains. Similar to that of sol-gel films, a minimum leakage current is achieved at 300°C just below the crystallization temperature because of the great reduction of growth defects.

An extended study on the sol-gel amorphous $Pb(Zr,Ti)O_3$ ferroelectric thin film was carried out by Deng *et al*. [22]. The thermal analysis results of PZT gel suggest a lower process temperature compared to that of the BST film. In general, the notable weight loss at a temperature below 300°C is attributed to the solvent evaporation and organic combustion. The exothermic peak around 350°C is attributed to decomposition and glass transition of the PZT gel, and the peak beyond 440°C is due to the crystallization of PZT grains. Similarly, pyrolyzed PZT thin films were annealed in a narrow temperature range just below the crystallization temperature at 410°C. The microstructural evolution in the films with the annealing temperature is

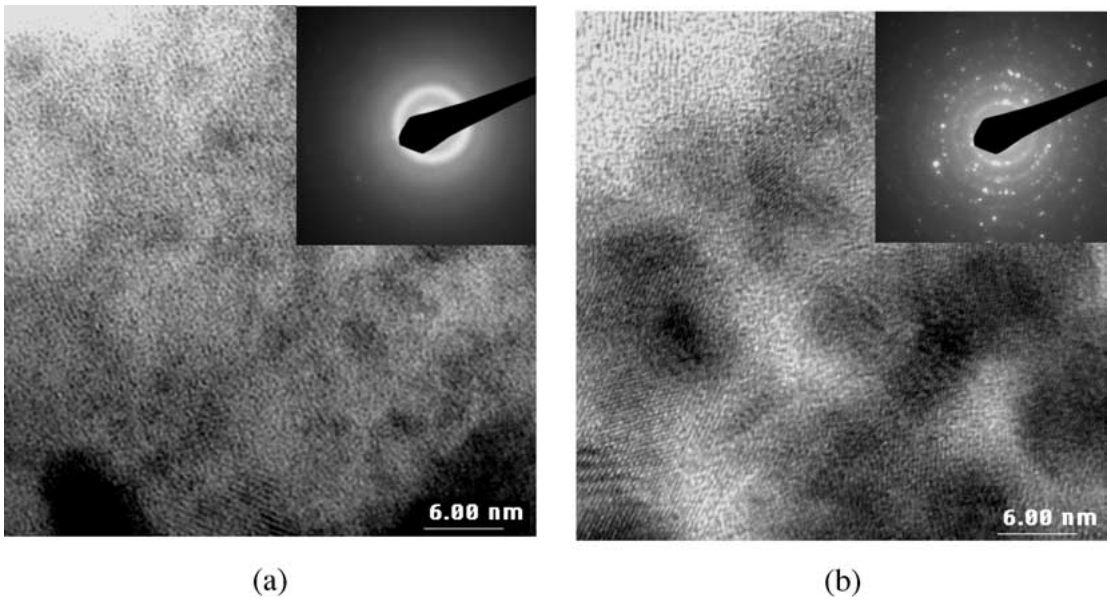

Figure 3 High-resolution TEM images of BST thin films annealed in air for 1 h at (a) 475°C and (b) 600°C [25].

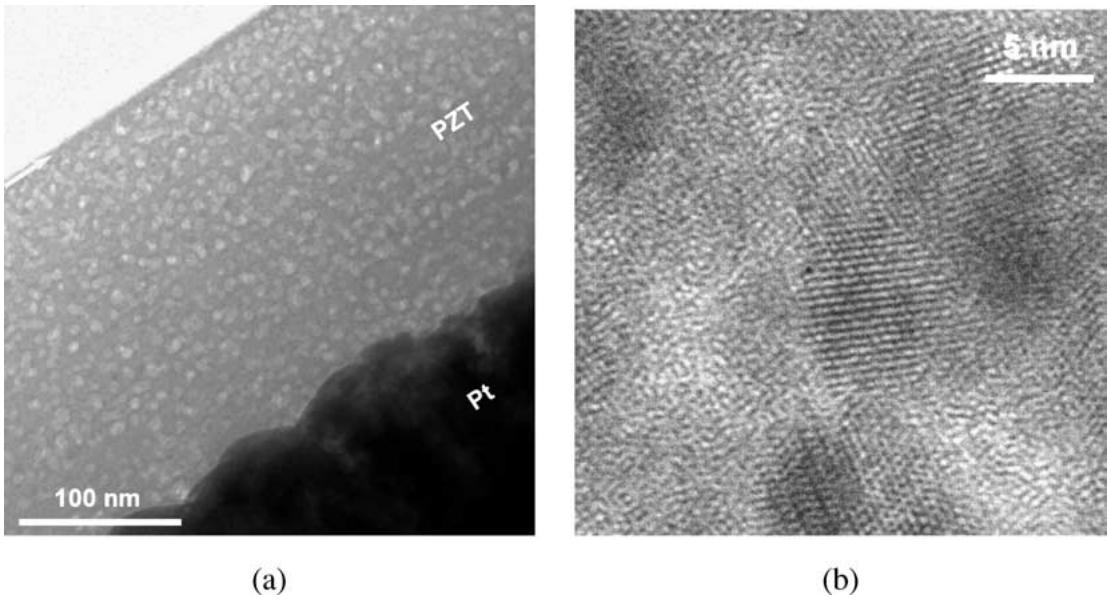

Figure 4 The cross-section view (a) and lattice image (b) of a PZT thin film annealed at 410°C [33].

clearly shown in their XRD [22] and TEM [33] studies. The film is amorphous in nature while annealed at 410°C. It exhibits a broad hump between 25° and 34°. Moreover, the metastable pyrochlore structure is developed at 490°C. However, the cross-section images shown in Fig. 4 [33] indicate that 410°C-annealed film is not completely in amorphous, but composed of a non-uniform amorphous matrix with embedded fine grains instead. Meanwhile, although the PZT gel was prepared with excess Pb, it has been identified that its surface layer is lead and oxygen deficient. Such microstructural feature is believed to significantly impact on the electric properties and gas sensitivity of the films. Deng [33] also depicted a consistent depth-profile using Raman spectroscopy, as shown in Fig. 5. He adopted a Raman spectra of 600°C-annealed PZT film as a reference curve, in which peaks at 204, 278, 331, 510,

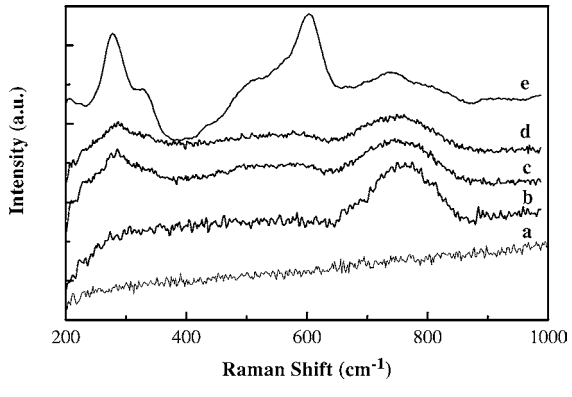

Figure 5 Raman spectra of amorphous BST thin film (a) and PZT thin films in different states. Curve (b) to (d) correspond to a PZT thin film annealed at 410°C, after 20 nm etching and after 40 nm etching, respectively. Curve (e) is for PZT thin film annealed at 600°C [33].

603, and 760 cm^{-1} correspond to E(2TO), B_1 + E, A_1(2TO), E(3TO), A_1(3TO), and E(3LO), respectively [34, 35]. After etching the Pb deficient surface layer, the 410°C-annealed PZT film displays a different spectrum from that of the as-deposited one, indicating different microstructural features between the surface layer and the interior region. The broadened peaks at 288 and 760 cm^{-1} are attributed to nano-sized grains in the films [36–39]. Also, similar impact of structural evolution on their leakage currents is observed in the sol-gel PZT thin films.

Moreover, the non-stoichiometric composition of amorphous ferroelectric films is another concern in fabrication, which might affect their electrical properties significantly. Zhu *et al*. [29] reported the influence of non-stoichiometric defects on the sol-gel amorphous BST films by varying the Ti concentration. The stoichiometric film with Ti (=1.00) has the lowest leakage current and the leakage current for the Ti (=1.02) film does not increase significantly. However, an obvious increase in leakage current is observed in the film with Ti (=1.04 and 0.98). Chen *et al*. [31, 32] detailed the influence of oxygen non-stoichiometric composition on *I-V* characteristics of sputtered BST thin films by varying the oxygen content in the sputtering atmosphere. Oxygen vacancies in these films are believed to be largely reduced with an increase of oxygen content. They conclude that the non-stoichiometric defect control in amorphous BST thin films is essential both in the bulk and at the interface for the practical application of the amorphous ferroelectric thin film hydrogen gas sensors. In sol-gel PZT films, it is revealed [22] that the leakage current is influenced by the Zr-to-Ti ratio, and the amorphous PZT 30/70 thin film with 2 mol% excess lead shows the lowest leakage current and highest dielectric breakdown field.

3. Gas sensing phenomenon of amorphous ferroelectric thin film capacitors

3.1. Temperature influence on the hydrogen sensing behaviors of amorphous ferroelectric thin film capacitors

The prototype amorphous ferroelectric hydrogen gas sensor is constructed in a capacitive configuration of Pd/ferroelectric thin film/Pt. In such a simple capacitive device, an amorphous ferroelectric thin film is fabricated on a Pt-coated silicon wafer as an insulating layer, and then a 50-nm catalytic layer Pd is deposited as a top electrode. The Pd metal layer dissociates the incoming hydrogen gas, transports hydrogen atoms to the metal-ferroelectric thin film interface, and adsorbs the hydrogen at this interface as detectable dipoles. Such hydrogen catalytic reaction is generally dominated by thermal equilibrium, suggesting that the operating temperature may affect their gas sensing behaviors significantly.

Tan *et al*. [40] described the influence of operating temperature on the gas sensing properties of the devices using a temperature sweeping technique. The gas sensitivity is defined by a difference between the leakage current in diluted hydrogen gas and in air, $I_{gas} - I_{air}$. Since I_{air} is subtracted as the background current, a clear picture of the effect of hydrogen gas on the change of current versus temperature is shown in Fig. 6. It is noted that this current change increases steadily up to around 250°C, then falls, and finally reaches a stable value at above 300°C. High sensitivity was observed in a temperature range of about 230–270°C. Tan *et al*. [40] explained this phenomenon in terms of the kinetic dissolution process of hydrogen in the Pd layer and thermally activated conduction at the Pd/BST interface. Under these assumptions, the kinetics for hydrogen dissolution at the interface between Pd and ferroelectric thin film can be described by

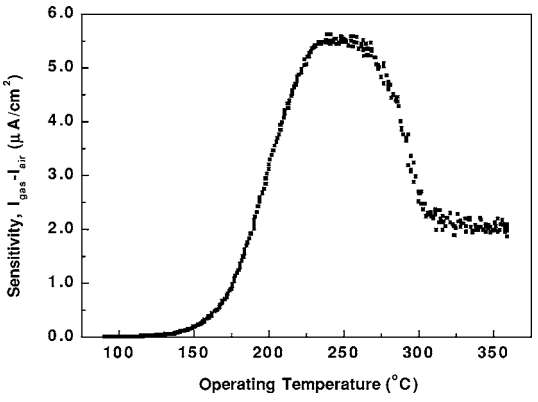

Figure 6 Hydrogen gas sensivity $I_{gas} - I_{air}$ versus operating temperature for an 125 nm thin film annealed at 475° in air for 1 h, biased at −0.25 V [40].

$$H_{2g} \underset{k_2}{\overset{k_1}{\rightleftharpoons}} 2H_a \underset{k_4}{\overset{k_3}{\rightleftharpoons}} 2H_i^+ + 2e^- \qquad (1)$$

where k_1, k_2, k_3 and k_4, are the rate constants of the reactions, *g*, *a* and *i* stand for the gaseous, adsorbed and interface species, respectively. By increasing the temperature, there is an increase in the dissociation of the H_2 molecules into H^+ ions and hence the increase of the accumulation of H^+ ions at the interface between the palladium layer and the amorphous BST film. On further increasing the temperature, more electrons in the film are thermally activated, neutralizing part of ionized H^+, and the hydrogen ions at the interface are also dislodged with increasing H^+ ion mobility. As an overall result, the change of dc current decreases above 270°C, and a stable state is reached at about 300°C as the final balance of these factors.

Similar results were reported by Chen *et al*. [32] and Deng *et al*. [22] in their studies of co-sputtered amorphous BST thin films and sol-gel amorphous PZT thin films, respectively. Comparatively, the co-sputtered amorphous BST thin film sensor exhibits a lower operating temperature. The highest gas sensitivity to hydrogen gas was obtained in the temperature range around 170–190°C. The sol-gel amorphous PZT thin film sensor also shows a lower operating temperature around 175°C. The lowering of operating temperature is believed to originate from the nature of ferroelectric thin films. For sputtered BST thin film, it might be attributed to the difficulty in control of the non-stoichiometric composition. For sol-gel PZT films,

some process-related issues should be considered, in particular, the off-stoichiometric interface and the formation of nano-sized grains.

3.2. Hydrogen sensitive *I-V* characteristics of amorphous ferroelectric thin film capacitors

It is found that amorphous ferroelectric thin film capacitors exhibit hydrogen-sensitive *I-V* characteristics, and the proton accumulation at the Pd/ferroelectric interface is believed to be the origin of this phenomenon [40]. Fig. 7 presents the *I-V* characteristics of a 125-nm-thick BST thin film annealed at 475°C, for both in air and in diluted hydrogen environment. Both of them exhibit a Schottky barrier emission conduction behavior owing to the Pd/BST contact. A striking feature is noted that the turn on applied voltage for the Schottky diode is tremendously shifted from about 5 V in air to about 0.5 V in 1000 ppm diluted hydrogen. However, the co-sputtered amorphous BST thin film capacitor shows a lower voltage shift of 0.6 V in the presence of same hydrogen gas [30]. Such a small voltage shift is related to the reduction of dissociated hydrogen atoms at the lower operating temperature, and in turn the weakening of the built-up space charge layer across the Pd/BST interface. Similarly, the voltage shift of PZT film is about 2.3 V at the same testing condition [22].

Fig. 8 demonstrates the influence of hydrogen concentration on the voltage shift of the BST devices [20, 40]. It clearly shows that under the negative bias all curves converge, manifesting no hydrogen gas effect under the negative bias. On the contrary, under the positive bias, all curves exhibit a Schottky barrier emission behavior, and the turn-on voltage consistently shifts to the left with the increase of hydrogen concentration. The plot of voltage shift versus hydrogen concentration in Fig. 8b indicates that there is a sharp slope in the low gas concentration range, and then a nearly linear region follows. Similarly, the PZT device also exhibits very high sensitivity to highly diluted hydrogen gas [22].

Such hydrogen-induced voltage shift is also dependent on their microstructural feature and stoichiometric composition. The microstructural influence on the gas sensitivity of BST thin film sensors has been addressed by Zhu *et al.* [25], and a blocking behavior of amorphous BST thin films for hydrogen diffusion was suggested. They compared the *I-V* characteristics of amorphous and crystalline BST thin film sensors in air and in 1000 ppm diluted hydrogen gas (Fig. 9). The amorphous film exhibits higher voltage shift value than that of the crystalline one annealed at 525°C. It is interesting that the hydrogen effect is observed both in the positive and negative bias regions for the crystalline film, whereas it just appears in the positive region for the amorphous one. It is hypothesized that amorphous BST films can effectively stop the protons at the Pd/BST interface, and thus enhance the interface dipole polarization potential. Such blocking behavior was also observed by Chen *et al.* [32] in their sputtered BST devices. In polycrystalline films, owing to introduction of protons in the film, the accumulation of protons at the interface is progressively decreased, and the hydrogen effects on *I-V* curves can be observed both in the positive and negative bias regions. Liedtke *et al.* [41], Ahn *et al.* [27], Iizuka *et al.* [26] and Baniecki *et al.* [28] have independently presented their experimental observations using SIMS, suggesting the presence of hydrogen atoms in crystalline BST thin films while annealing in hydrogen-containing atmosphere.

The influence of non-stoichiometric composition was reported by Zhu *et al.* [29] by varying Ti concentration in amorphous BST films. Fig. 10 illustrates the

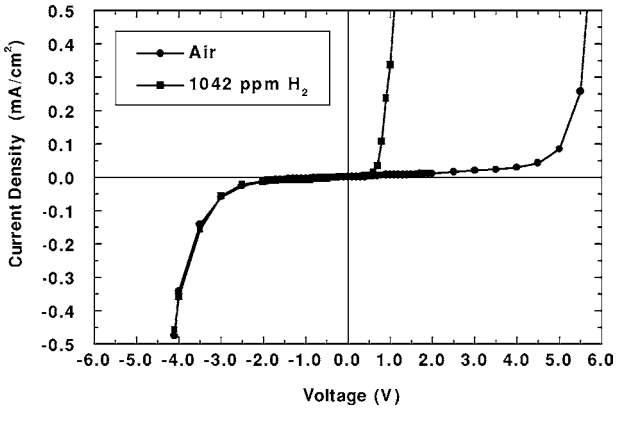

Figure 7 *I-V* characteristics of a sol-gel amorphous BST thin film capacitive device in air and in 1042 ppm diluted hydrogen gas, measured at 250°C [40].

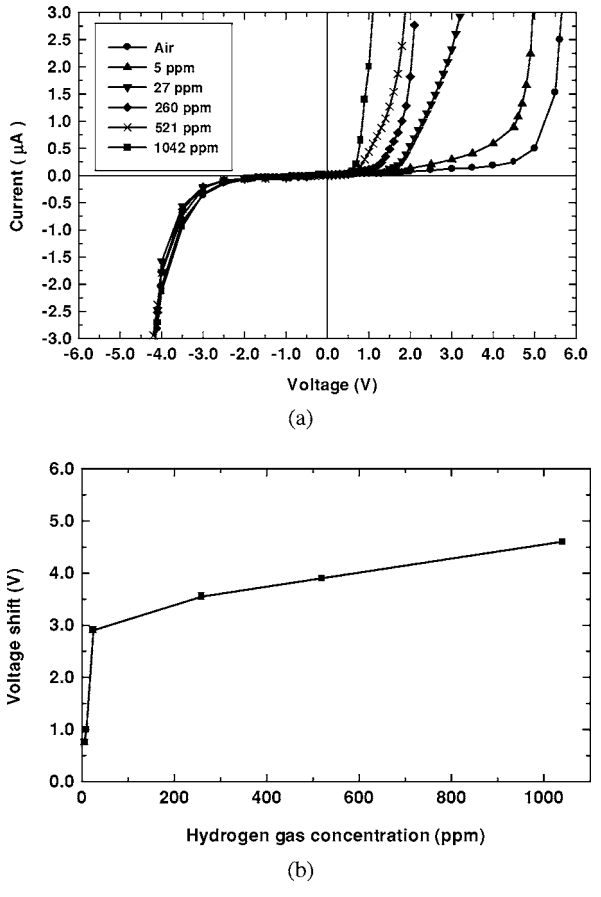

Figure 8 *I-V* characteristic of a sol-gel amorphous BST thin film gas sensor as a function of hydrogen concentration (a) and corresponding voltage shift value of the device (b) [20].

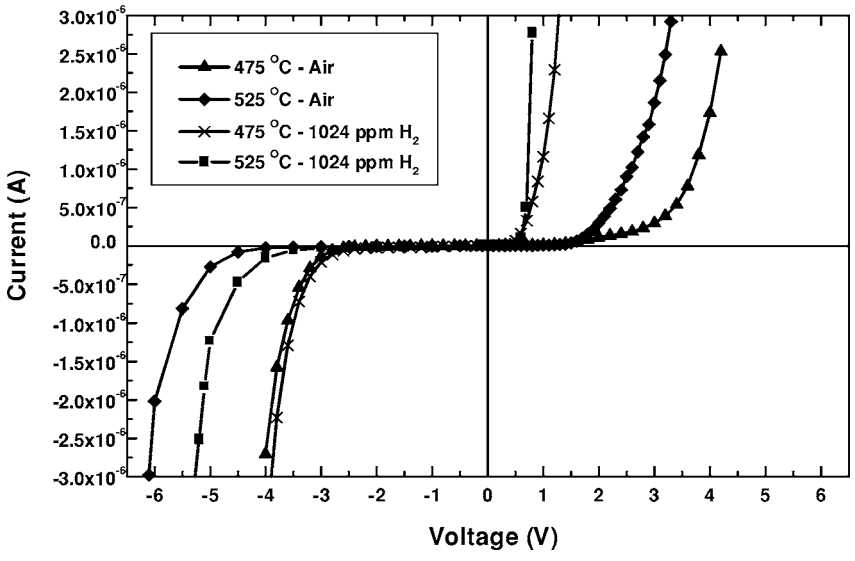

Figure 9 Microstructural influence on the hydrogen sensitive *I-V* characteristics of sol-gel BST thin films annealed at 475°C and 525°C [25].

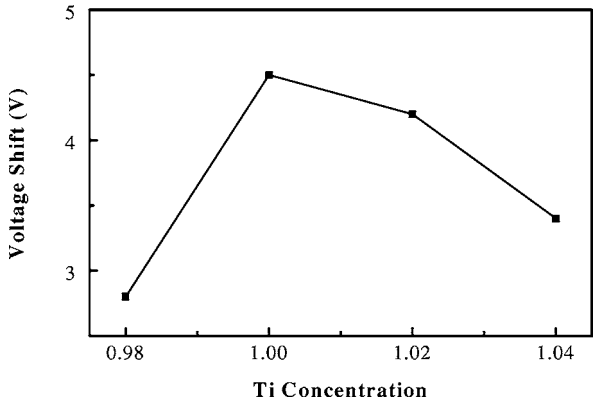

Figure 10 Turn-on voltage shift of sol-gel amorphous BST gas sensors in 1000 ppm diluted hydrogen gas versus Ti concentration [29].

turn-on voltage shift of sol-gel amorphous BST films with different Ti concentrations, measured in 1000-ppm hydrogen gas. It evidently indicates the correlation between the gas sensitivity of the devices and their conduction behaviors. The stoichiometric BST thin films, which has the lowest leakage current, yields a turn-on voltage value of 4.5 V. In those non-stoichiometric films showing high electric conduction, the probability of recombination of protons with electrons increases and the built-up potential at the interface becomes lower. In amorphous PZT films, it is revealed [22] that the voltage shift is also dependent on the Zr/Ti ratio.

4. Hydrogen gas sensing mechanism of amorphous ferroelectric thin film sensors

Exploring the amorphous ferroelectric thin films for hydrogen detection, the physical nature of hydrogen sensing phenomenon is of interest for the fundamental understanding of ferroelectric thin films. Several papers focusing on this aspect have been published recently, starting from the conduction mechanisms of amorphous ferroelectric thin films and impedance measurements.

4.1. Conduction mechanism in amorphous ferroelectric thin films

Similar to that of polycrystalline ferroelectric thin film capacitors discussed in literature [42], the conduction mechanism of sol-gel amorphous BST and PZT thin films has been systematically studied by Zhu *et al*. [29] and Deng *et al*. [33] recently. The favored mechanisms with the noble metal Pd electrode are Schottky-barrier emission for BST films and space charge limited current (SCLC) for PZT films, respectively.

In the Schottky emission theory, the leakage current density I_{SK} can be expressed as

$$\ln\left(\frac{I_{SK}(V)}{T^2}\right) = \ln A^* + \frac{\sqrt{\frac{q^3E}{4\pi\varepsilon_0\varepsilon_i}} - q\varphi_B}{k_B T}, \quad (2)$$

where A^* is the effective Richardson constant, φ_B the potential height at the surface, ε_i the dynamic dielectric constant, q unit charge, k_B Boltzmann constant, T temperature, and E the applied electric field. The sol-gel amorphous BST thin films exhibit linear $I \sim \sqrt{E}$ and $\ln(\frac{I}{T^2})$ versus $\frac{1}{T}$ characteristics, confirming that their leakage current is dominated by the Schottky emission mechanism [29, 43]. The Schottky barrier height is derived to be about 0.98 eV, and the dynamic dielectric constant is around 1.6, corresponding to an optical refractive index of about 1.3. It is consistent with that of 1.74 in the infrared region for the sol-gel amorphous $La_{0.003}Ba_{0.7}Sr_{0.3}TiO_3$ thin film by Suzuki and coworkers [44]. The corresponding value in ellipsometric analysis is estimated to be 1.77 at a wavelength of 900 nm. In contrary, the value derived from Poole-Frenkel emission is about 5, indicating that Poole-Frenkel emission is ruled out in principle.

In SCLC dominated conduction, the space-charge-limited current could be written as [45, 46]

$$I \propto \frac{V^{m+1}}{d^{2m+1}}, \quad (3)$$

where d is the film thickness, V applied voltage, and m the index indicating the trap distribution ($m = 1$ for trap

with single discrete energy level and $m > 1$ for non-discrete traps). For amorphous PZT films, the m value derived is 3.1, 2.8, and 2.6 at 155°C, 175°C and 190°C, respectively [33]. The values exceeding 1 indicate the energy levels of the traps in an amorphous PZT are non-discrete owing to its microstructural feature with nano-sized grains embedded in the amorphous matrix and the lead-deficient surface layer.

4.2. Impedance analysis

An important experimental approach to clarify the hydrogen gas sensing mechanism of amorphous ferroelectric thin film capacitors was performed by Zhu *et al*. [24] and Deng *et al*. [33] using the impedance analysis technique. The experimental results evidently suggest a proton-blocking model at the interface between the Pd layer and the amorphous ferroelectric thin film in the presence of hydrogen.

The initial investigation on frequency spectra of sol-gel amorphous BST thin films [20] suggests a Debye dielectric behavior. Recently Deng *et al*. [33] found that the impedance spectra of amorphous BST thin films show a deviated behavior from the ideal Debye response at a higher temperature range, as shown in Fig. 11. The depressed semicircles indicate a deviation from the ideal Debye relaxation, and it is usually modeled by a so-called constant phase element (CPE) or non-Debye capacitor instead [47, 48]. The CPE impedance is presented as

$$Z_{\mathrm{CPE}}(\omega) = C^{-1}(j\omega)^{-\mathrm{n}}, \tag{4}$$

and n is usually less than 1 depending on the depression of the arc. The circuit simulation shows that the depression parameter n is about 0.98 for the bulk film in the entire testing temperature range, suggesting a *quasi*-Debye relaxation behavior. For the interface between Pd layer and amorphous BST film, a depression parameter n of 0.9 is estimated, attributed to a distributed space-charge region at the interface.

It is interesting that the hydrogen concentration has a significant impact on the impedance spectra of the Pd/amorphous BST/Pt capacitive gas sensor at 190°C, shown in Fig. 12 [24]. The equivalent circuit simulation indicates that the n_{B} value of the amorphous BST thin film bulk is approximated to be 1 independent of the hydrogen concentration, indicating a *quasi*-Debye relaxation behavior. Meanwhile, the interface capacitance C_{I}

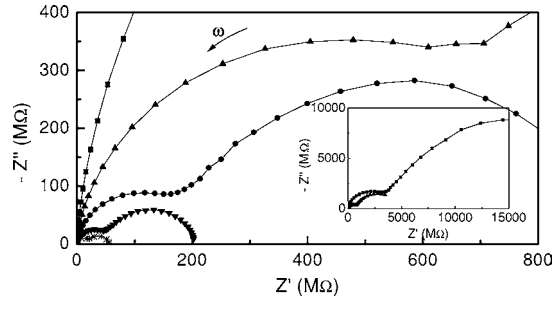

Figure 11 Impedance spectra of an amorphous BST thin film at different temperatures in air: 155°C (■), 175°C (▲), 190°C (●), 208°C (▼), and 225°C (⋆). The inset plot is the experimental data at 155 and 175°C [33].

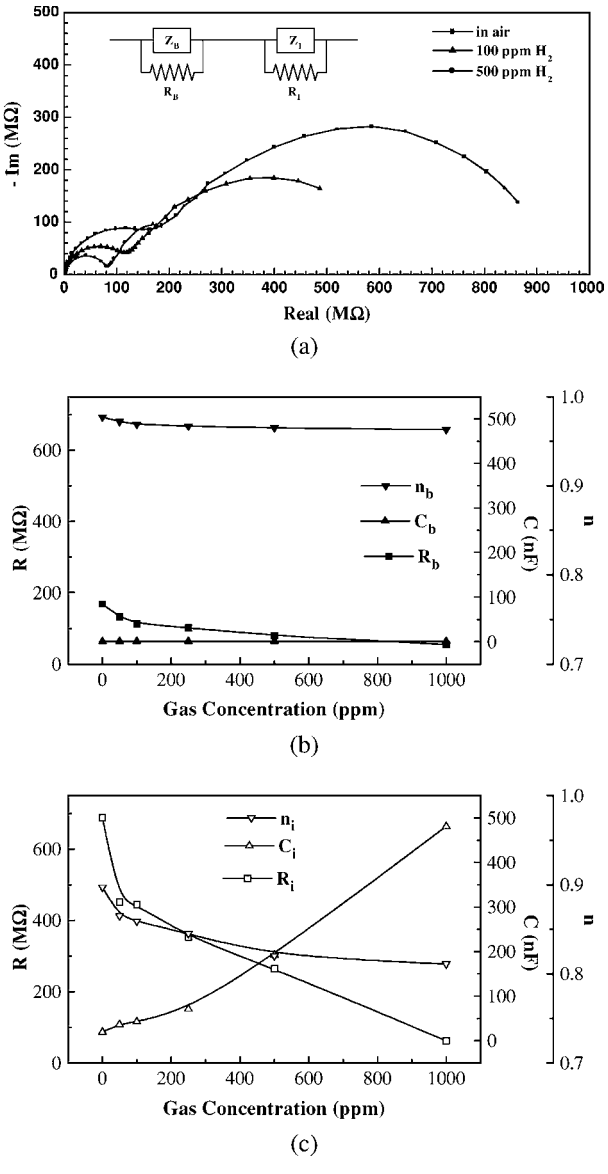

Figure 12 (a) Influence of hydrogen concentration on the impedance spectra of a sol-gel amorphous BST thin film gas sensor operated at 190°C and the equivalent circuit, (b) and (c) are the estimated circuit element parameters by simulation [33].

increases significantly with increasing hydrogen concentration, interpreted by the proton accumulation at the Pd/BST interface. The accumulated protons can lower the contact potential of the interface, and in turn affect the resistance of R_{B} and R_{I}. The n_{I} value decreases with the increase of hydrogen concentration, indicating a deviation from the Debye-like relaxation behavior at the Pd/BST interface in the presence of hydrogen. The semicircle at the low frequencies indicates that no infinite length Warburg element occurs even at the frequency as low as 1 mHz. In particular, the Warburg element with an n value of 0.5 usually stands for a diffusion process, appearing as a linear curve in a Cole-Cole plot. It suggests that the penetration of protons into the BST film in the presence of hydrogen can be clearly ruled out, and instead, the protons are blocked at the Pd/BST interface.

A similar impedance spectrum was also observed in a Pd/amorphous PZT/Pt capacitor by Deng [33], as shown in Fig. 13. Circuit simulation suggests that with

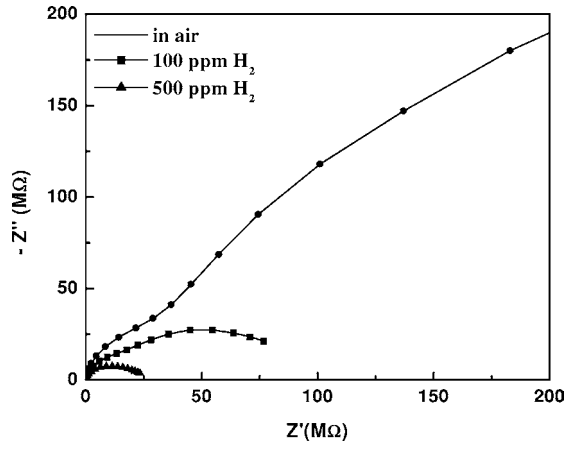

Figure 13 Impedance spectra of a sol-gel amorphous PZT thin film gas sensor in different hydrogen concentrations at 175°C [33].

an increase of hydrogen concentration, the increased interface capacitance C_I may originate from the additional polarization potential at the interface, then R_B and R_I are affected, and their *I-V* characteristics are altered. However, the increase of C_I for PZT films in hydrogen is much smaller than that for BST. It indicates a weakened accumulation of protons at the Pd/PZT interface, which results in smaller dipole polarization potential and lower hydrogen sensitivity.

4.3. Model of hydrogen gas sensing

The hydrogen-sensing model, schematically shown in Fig. 14, was initially proposed by Zhu, Tan and Yao [20] in 1998, to explain the effect of hydrogen gas on the enhanced interfacial polarization potential. In this model, when hydrogen molecules reach the Pd surface, they become hydrogen atoms due to the catalytic effect of palladium metal to hydrogen. The hydrogen atoms are then ionized under a positive bias, migrate to the interface between the Pd metal layer and the amorphous ferroelectric BST film. It is assumed that protons are blocked at this interface. This accumulation of positive protons at the interface results in the build-up of charges that in turn causes a dipole polarization potential at the interface. While reversing the bias voltage, protons are

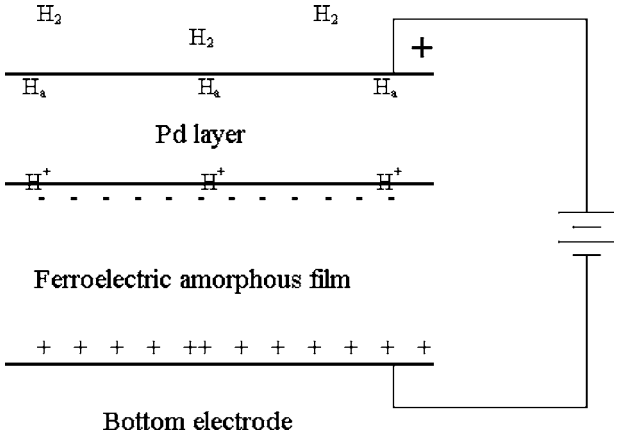

Figure 14 Schematic model to explain the enhanced hydrogen induced interfacial polarization potential between the Pd layer and the amorphous ferroelectric BST thin film [20].

driven out from the Pd layer, and consequently no dipole polarization potential can be built up at the Pd/BST interface. In this model, the proton-blocking hypothesis of amorphous BST thin films has been confirmed in their experimental studies both by *I-V* characteristics [20, 40] and by impedance analysis [24].

A mathematical description of this proton-induced space-charge polarization potential was demonstrated by Tan *et al*. [40]. It is assumed that the current flowing through the device is a dominant process of electron transport over the potential barrier between the BST film and the Pd metal. Then the *I-V* characteristic is expressed in terms of the thermionic emission diffusion theory by Crowell and Sze [48]

$$I(V) = A^*T^2 \exp\left(-\frac{q\phi_{BO}}{kT}\right) \times \left[\exp\left(\frac{q\Delta\phi + qV}{kT}\right) - 1\right], \quad (5)$$

where ϕ_{BO} is the zero-field asymptotic barrier height, $\Delta\phi$ the Schottky barrier lowering, V the applied forward voltage and A^* the effective Richardson constant. In their consideration of hydrogen gas sensing, they inferred that the term $\Delta\phi$ is dominant due to the accumulation of protons at the interface that resulted in an electric potential build-up, induced a very large polarization across the BST film and caused the barrier height lowering. This effect is analogous to the image force-induced lowering of the potential barrier because of the interface states. Equation 5 can be rewritten as

$$I(V) = A^*T^2 \exp\left(-\frac{q\phi_{BO}}{kT}\right) \times \left[\exp\left(\frac{q\Delta V_H + qV_{FH}}{kT}\right) - 1\right], \quad (6)$$

where ΔV_H is the lowering of the barrier height in the presence of hydrogen gas and V_{FH} the applied forward voltage in the hydrogen environment.

Based on the interface-blocking model, a hydrogen potential energy diagram of the Pd/BST interface was described schematically by Chen *et al*. [32] and Zhu *et al*. [24], analogous to the Pd/SiO_2 interface in Pd/MOS devices, shown in Fig. 15. In the presence of hydrogen, the hydrogen coverage equilibrium between the surface and the interface is achieved and described by

$$\frac{\theta_i}{1-\theta_i} = e^{-\frac{\Delta H_s - \Delta H_i}{kT}} \frac{\theta_s}{1-\theta_s}, \quad (7)$$

where θ_i is the hydrogen coverage at the Pd/BST interface, ΔH_i and ΔH_s the heat of adsorption at the Pd/BST interface and at the Pd surface, respectively. When a new dipole forms at the interface, its charges feel the repulsive electrostatic field from the already existing charge sheets. With the two-dimensional dipole assumption, the potential energy change, ΔV, caused by the hydrogen induced build-up space charge is

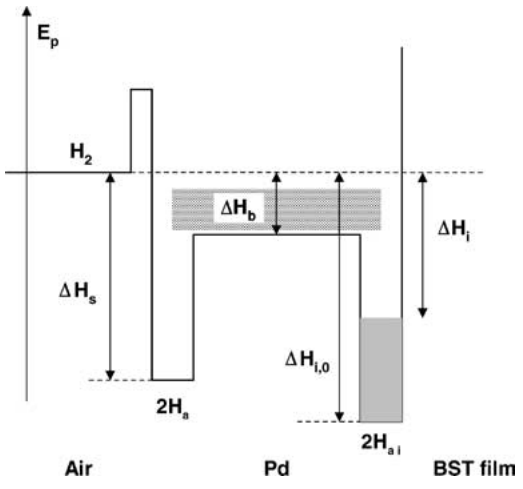

Figure 15 Schematic hydrogen potential energy diagram of the Pd/BST interface [24].

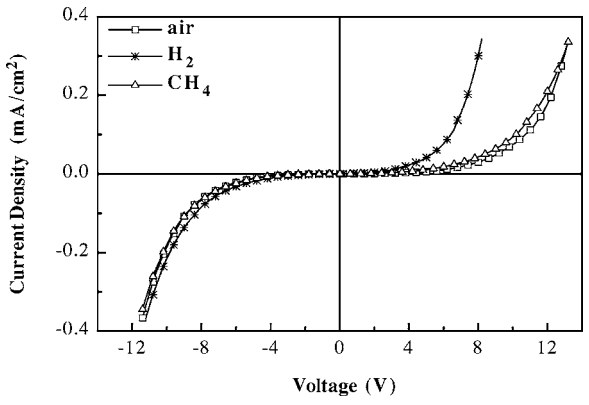

Figure 16 Gas-selective *I-V* characteristics of an amorphous BST thin film gas sensor, measured in 1000-ppm hydrogen and 1000-ppm methane diluted in air at 190°C [33].

determined by the hydrogen coverage at the interface,

$$\Delta V = \frac{n_{\mathrm{i}}\mu}{\varepsilon}, \tag{8}$$

where n_{i} is the hydrogen concentration at the interface, μ the effective dipole moment, and ε the permittivity. An effective reduction of the adsorption heat is presented by

$$\Delta H_{\mathrm{i}} = \Delta H_{\mathrm{i},0} - q\Delta V = \Delta H_{\mathrm{i},0} - \frac{q\mu n_{\mathrm{i}}}{\varepsilon}, \tag{9}$$

where $\Delta H_{\mathrm{i},0}$ is the initial adsorption energy. When the interface adsorbate coverage becomes high enough so that the adsorption energy is reduced to that of the Pd bulk, ΔH_{b}, a significant amount of hydrogen will also start to accumulate in the bulk. Therefore, a practical upper limit exists for the sensor response. This limit is reached at a so-called maximum hydrogen concentration $n_{\mathrm{i,p}}$ at the interface

$$n_{\mathrm{i,p}} \approx (\Delta H_{\mathrm{i},0} - \Delta H_{\mathrm{b}})\frac{\varepsilon}{q\mu}. \tag{10}$$

This equation indicates that the high permittivity of the amorphous ferroelectric thin film, 14 for BST and 22 for PZT, will increase the concentration of the accumulated protons at the Pd/amorphous ferroelectric interface compared to 3.9 of silicon dioxide, and as a direct result, the built-up space charge is largely improved. It also explains why the hydrogen gas induced interface polarization potential is greatly enhanced in a Pd/amorphous ferroelectric film/Pt hydrogen gas sensing capacitive device.

5. Gas sensing response of amorphous ferroelectric thin film sensors

At present, the prototype gas sensor based on amorphous ferroelectric thin films is fabricated in a capacitive device with a hot stage. The practical performance of these ferroelectric thin film capacitive sensors is investigated in terms of selectivity, transient response and sensitivity.

The amorphous ferroelectric thin film gas sensor is found to have good selectivity to hydrogen. Zhu *et al*. [21] tested the sensitivity of an amorphous BST thin film capacitor in 1000-ppm hydrogen, ethanol and carbon monoxide gases. The BST capacitor shows the distinct selectivity toward hydrogen gas over ethanol and carbon monoxide gases. Deng [33] also compared the *I-V* curves of an amorphous BST gas sensor in air-diluted 1000-ppm hydrogen and methane at 190°C, shown in Fig. 16. A negligible shift of *I-V* curve is observed in methane, indicating an excellent selectivity to hydrogen gas.

Their transient response is mainly dependent on the operating conditions and the chemical reaction in Pd metal. Tan *et al*. [40] studied the transient response of an amorphous BST thin film capacitor using a current-time response measurement. The current rose from near zero to around 27 nA at 250°C while introducing the hydrogen gas, and fell back after turning off. The *dc* bias voltage significantly influences the transient response both in response phase and in recovery phase, and the best transient response of several minutes was found to occur at around −0.2 V. The operating temperature also affects the transient response of BST gas sensors considerably due to the involved kinetic processes for the Pd/BST hetero-structure. An improved transient response of 19 s to 100-ppm hydrogen gas at 190°C was reported by Deng *et al*. [49], applying a *dc* bias voltage of +0.2 V.

Meanwhile, the diluted gas also exhibits a notable influence on the transient response of the amorphous ferroelectric gas sensors. Deng *et al*. [49] compared the transient responses of an amorphous BST gas sensor in 100-ppm hydrogen diluted in air and in nitrogen, shown in Fig. 17. In response phase, a rising time of 9 s for the nitrogen diluted gas and that of 19 s for the air-diluted gas are measured. In recovery phase, the corresponding time is 270 s and 130 s, respectively. He correlated this phenomenon with the chemical reactions in the Pd/BST hetero-structure. The presence of oxygen impacts significantly on the chemical reactions described in Equation 1, and leads to the formation of water layer on the Pd surface. In the response phase, hydrogen penetrating into the catalytic Pd metal is impeded owing to the adsorption of oxygen and its reaction with hydrogen,

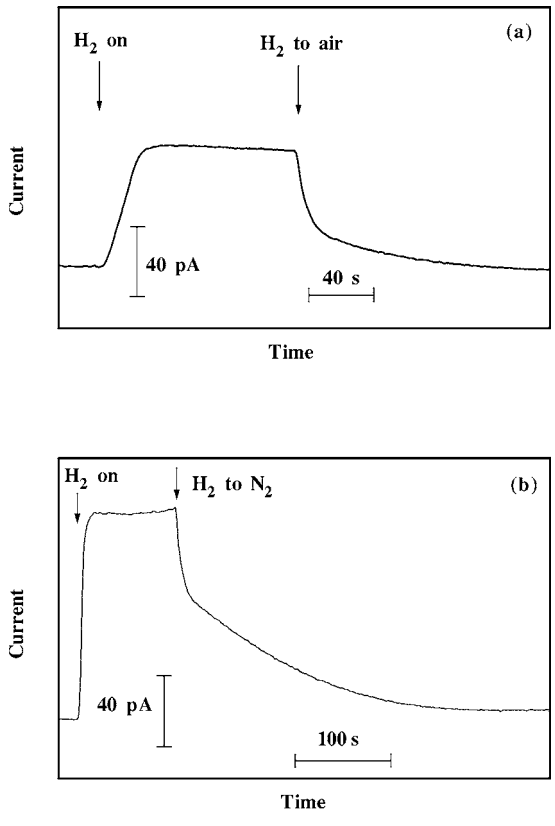

Figure 17 Transient response and recovery of an amorphous ferroelectric BST gas sensor in 100 ppm hydrogen gases diluted in air (a) and in nitrogen (b) [49].

and consequently the transient response is slower. On the other hand, the formation of the water layer accelerates the recovery process in the presence of oxygen after turning off the hydrogen. Similar transient behavior of an amorphous PZT thin film gas sensor was also observed by Deng *et al*. [33]. The rising time and recovery time to 100-ppm air-diluted hydrogen gas are 120 and 145 s, respectively. Its transient time is slower than that of the BST gas sensor.

6. Summary

In this review, we summarize recent research progresses on the hydrogen-sensitive amorphous ferroelectric thin film capacitors, and in particular stress on the feasibility to fabricate high-sensitivity hydrogen gas detectors using ferroelectric thin films in the amorphous state. An important breakthrough in solid state hydrogen sensors was achieved by Zhu *et al.* [20, 21] in 1998 using a sol-gel amorphous BST thin film, which displays a large voltage shift of 4.5 V in 1000 ppm diluted hydrogen gas. Such promising progress was extended to other ferroelectric thin films successively, employing an amorphous PZT thin film. However, since it is still under development stage, the prototype devices are mainly fabricated based on a simple capacitive configuration. The research activities in the past five years cover the fabrication and fundamental properties of amorphous ferroelectric thin films, transient response of the devices and their gas sensing mechanisms.

Several process parameters are correlated with their microstructural features and electrical measurements. The elimination of non-stoichiometric defects is essential to achieve low leakage current and high breakdown field both in sputtering and in sol-gel processes. The appearance of nano-grains and incompletely developed grain-boundaries usually lead to associated electronic trapped charges, and in turn deteriorate their electrical properties. The merit using amorphous BST thin films is that the amorphous structure can block protons effectively at the Pd/BST interface based on the electric measurements, whereas the protons have been proved to penetrate into polycrystalline BST thin films.

The sensitivity of amorphous ferroelectric thin film hydrogen detectors is dominated by their electrical properties and the catalytic effect of the Pd layer. The associated electronic defects in amorphous ferroelectric thin films generally lower the gas sensitivity due to the thermal-activation process. The transient response principally depends on the kinetic process of hydrogen dissolved into the Pd layer and associated chemical reactions.

The hydrogen sensing mechanism is attributed to the build-up of a hydrogen induced polarization potential at the interface between Pd layer and amorphous ferroelectric thin film. The proton accumulation at the interface is greatly enhanced owing to the high dielectric constant of amorphous ferroelectric thin films, and in turn excellent hydrogen sensitivity is observed. Compared to the existing technologies, the ferroelectric thin film in amorphous state is regarded as the most promising candidate for the prospective hydrogen detecting application with high sensitivity, and in turn the monolithic silicon-based ferroelectric hydrogen detectors will be developed in the near future.

References

1. M. C. MADOU and S. R. MORRISON, "Chemical Sensing with Solid State Devices" (New York, Academic Press, 1989).
2. A. MANDELIS and C. CHRISTOFIDES, "Physics, Chemistry and Technology of Solid State Gas Sensor Devices" (Wiley Interscience, 1993).
3. K. I. LUNDSTRÖM, S. SHIVARAMAN, C. SVENSSON and L. LUNDKVIST, *Appl. Phys. Lett.* **26** (1975) 55.
4. K. I. LUNDSTRÖM, S. SHIVARAMAN and C. SVENSSON, *J. Appl. Phys.* **46** (1975) 3876.
5. K. I. LUNDSTRÖM and C. SVENSSON, "Gas-Sensitive Metal Gate Semiconductor Devices" in "Solid State Chemical Sensors," edited by J. Janata and R. J. Huber (New York, Academic Press, 1985) p. 1.
6. M. ERIKSSON, I. LUNDSTRÖM and L. G. EKEDAHL, *J. Appl. Phys.* **82** (1997) 3143.
7. J. FOGELBERG, M. ERIKSSON, H. DANNETUN and L. G. PETERSSON, *ibid.* **78** (1995) 988.
8. J. FOGELBERG and L.-G. PETERSSON, *Surf. Sci.* **350** (1996) 91.
9. K. DOBOS, M. ARMGARTH, G. ZIMMER and I. LUNDSTRÖM, *IEEE Trans. Electron Devices* **31** (1984) 508.
10. S. OKUYAMA, N. TAKINAMI, Y. CHIBA, S. OHSHIMA and S. KAMBE, *J. Appl. Phys.* **76** (1997) 231.
11. S. OKUYAMA, K. UMEMOTO and K. OKUYAMA, *Jpn. J. Appl. Phys.* **36** (1997) 1228.
12. A. ARBAB, A. SPETZ and I. LUNDSTRÖM, *Sensors and Actuators* B **15/16** (1993) 19.
13. L. Y. CHEN, G. W. HUNTER, P. G. NEUDECK, G. BANSAL, J. B. PETIT and D. KNIGHT, *J. Vac. Sci. Tech.* A **15** (1997) 1228.
14. A. BARANZAHI, A. L. SPETZ, B. ANDERSON and I. LUNDSTRÖM, *Sensors and Actuators* B **26/27** (1996) 165.

15. S. BASU and A. DUTTA, *ibid.* **22** (1994) 83.
16. H. KOBAYASHI, K. KISHIMOTO and Y. NAKATO, *Surf. Sci.* **306** (1994) 393.
17. W. P. KANG and Y. GÜRBÜZ, *J. Appl. Phys.* **75** (1994) 8175.
18. W. P. KANG, Y. GURBUZ, J. L. DAVIDSON and D. V. KERNS, *Sensors and Actuators B* **24/25** (1995) 421.
19. Y. GURBUZ, W. P. KANG, J. L. DAVIDSON, D. L. KINSER and D. V. KERNS, *ibid.* **33** (1996) 100.
20. W. G. ZHU, O. K. TAN and X. YAO, *J. Appl. Phys.* **84** (1998) 5134.
21. W. ZHU, O. K. TAN, M. S. TSE and X. YAO, *J. Korean Phys. Soc.* **32** (1998) s1778.
22. J. DENG, W. ZHU and O. K. TAN, *Sensors and Actuators* B **77** (2001) 416.
23. W. G. ZHU, O. K. TAN, J. DENG and X. YAO, *Ferroelectrics* **232** (1999) 165.
24. W. G. ZHU, J. DENG, O. K. TAN and X. F. CHEN, *Asian Ceram. Sci. Electr. I: Key Eng. Mater.* **7** (2002) 183.
25. W. G. ZHU, O. K. TAN, Q. YAN and J. T. OH, *Sensors & Actuators* B **65** (2000) 366.
26. T. IIZUKA, K. ARITA, I. YAMAMOTO, S. YAMAMICHI, H. YAMAGUCHI, T. MATSUKI, S. SONE, H. YABUTA, Y. MIYASAKA and Y. KATO, *Jpn. J. Appl. Phys.* **39** (2000) 2063.
27. J. H. AHN, P. C. MCINTYRE, L. W. MIRKARIMI, S. R. GILBERT, J. AMANO and M. SCHULBERG, *Appl. Phys. Lett.* **77** (2000) 1378.
28. J. D. BANIECKI, R. B. LAIBOWITZ, T. M. SHAW, C. PARKS, J. LIAN, H. XU and Q. Y. MA, *J. Appl. Phys.* **89** (2001) 2873.
29. W. G. ZHU, O. K. TAN, J. DENG and J. T. OH, *J. Mater. Res.* **15** (2000) 1291.
30. O. K. TAN, X. F. CHEN and W. G. ZHU, *Ferroelectrics* **225** (1999) 295.
31. X. F. CHEN, W. G. ZHU, O. K. TAN and M. S. TSE, *ibid.* **232** (1999) 71.
32. X. F. CHEN, W. G. ZHU and O. K. TAN, *Mater. Sci. Eng.* B **77** (2000) 177.
33. J. DENG, "Ferroelectric Thin Films for Hydrogen Gas Sensor," PhD thesis of Nanyang Tech. Univ., Singapore, 2001.
34. Y. IKEUCHI, S. KOJIMA and T. YAMAMOTO, *Jpn. J. Appl. Phys.* **36** (1997) 2985.
35. Y. I. YUZYUK, R. FARHI, V. L. LORMAN, L. M. RABKIN, L. A. SAPOZHNIKOV, E. V. SVIRIDOV and I. N. ZAKHARCHENKO, *J. Appl. Phys.* **84** (1998) 452.
36. W. ZHU, Z. Q. LIU, W. LU, M. S. TSE, H. S. TAN and X. YAO, *ibid.* **79** (1996) 4283.
37. B. MIHAILOVA, S. STOYANOV, V. GAYDAROV, M. GOSPODINOV and L. KONSTANTINOV, *Solid State Commun.* **103** (1997) 623.
38. M. H. LEE and B. C. CHOI, *J. Amer. Ceram. Soc.* **74** (1991) 2309.
39. D. BERSANI, P. P. LOTTICI, A. MONTENERO, S. PIGONI and G. GANAPPI, *J. Mater. Sci.* **31** (1996) 3153.
40. O. K. TAN, W. G. ZHU, M. S. TSE and X. YAO, *Mater. Sci. Eng.* B **58** (1999) 221.
41. R. LIEDTKE, M. GROSSMANN and R. WASER, *Appl. Phys. Lett.* **77** (2000) 2045.
42. J. F. SCOTT, *Ferr. Rev.* **1** (1998) 1.
43. J. DENG, X. F. CHEN, O. K. TAN and W. G. ZHU, "International Conf. on Mass and Charge Transport 2000" (Venice, Italy, 2000).
44. I. SUZUKI, M. EJIMA, K. WATANAKE, Y. XIONG and T. SAITOH, *Thin Solid Films* **313/314** (1998) 214.
45. M. A. LAMPERT and P. MARK, "Current Injection in Solids" (New York, Academic Press, 1970).
46. C. HAMANN, H. BURGHARDT and T. FRAUENHEIM, "Electrical Conduction Mechanisms in Solids" (Berlin, Deutscher Verlag der Wissenschaften, 1988).
47. A. K. JONSCHER, "Dielectric Properties: A Review of Data and Their New Interpretation" (New York, Academic Press, 1980).
48. C. R. CROWELL and S. M. SZE, *Solid-State Electr.* **9** (1966) 1035.
49. J. DENG, W. G. ZHU, O. K. TAN, X. F. CHEN and X. YAO, *Ferroelectrics* **263** (2001) 181.

Received 27 March
and accepted 26 July 2003